

Dynamical quantum phase transitions in the one-dimensional extended Fermi-Hubbard model

Juan José Mendoza-Arenas

*Departamento de Física, Universidad de los Andes, A.A. 4976, Bogotá D. C., Colombia and
H.H. Wills Physics Laboratory, University of Bristol, Bristol BS8 1TL, UK*

(Dated: September 23, 2021)

Based on tensor network simulations, we discuss the emergence of dynamical quantum phase transitions (DQPTs) in a half-filled one-dimensional lattice described by the extended Fermi-Hubbard model. Considering different initial states, namely noninteracting, metallic, insulating spin and charge density waves, we identify several types of sudden interaction quenches which lead to dynamical criticality. In different scenarios, clear connections between DQPTs and particular properties of the mean double occupation or charge imbalance can be established. Dynamical transitions resulting solely from high-frequency time-periodic modulation are also found, which are well described by a Floquet effective Hamiltonian. State-of-the-art cold-atom quantum simulators constitute ideal platforms to implement several reported DQPTs experimentally.

I. INTRODUCTION

In spite of being the object of intense research for several decades, interacting many-body quantum systems continue posing some of the most exciting and challenging problems in modern physics. Key examples manifest during their unitary dynamics resulting from nonequilibrium setups such as sudden quenches, where fundamental phenomenology including thermalization [1–5] and transport of conserved quantities [6–8] emerges. The understanding of these problems has received an enormous boost largely due to the development of powerful numerical methods [9–11], and due to the implementation of quantum simulators which allow for exquisite unprecedented control of the degrees of freedom of many-body systems [12–14].

A fascinating effect identified within this combined effort, known as dynamical quantum phase transitions (DQPT), results from taking general ideas of quantum criticality to the nonequilibrium scenario [15, 16]. This concept relies on the return (or Loschmidt) amplitude of the evolved state $|\psi_0(t)\rangle$ of a quantum system to its initial state $|\psi_0\rangle$,

$$\mathcal{G}(t) = \langle \psi_0 | \psi_0(t) \rangle = \langle \psi_0 | e^{-iHt} | \psi_0 \rangle, \quad (1)$$

during the dynamics arising from a sudden quench. Here $|\psi_0\rangle$ is the ground state of a Hamiltonian H_0 , and H is the post-quench Hamiltonian. The Loschmidt amplitudes have been argued to be similar to canonical partition functions in equilibrium [15]. Namely, for a system of $L \gg 1$ sites, the associated Loschmidt echo $\mathcal{L}(t)$ has a dependence with L of the form

$$\mathcal{L}(t) = |\mathcal{G}(t)|^2 = e^{-L\lambda(t)} \quad (2)$$

with $\lambda(t)$ a real-valued (intensive) rate function which is obtained in the thermodynamic limit as

$$\lambda(t) = - \lim_{L \rightarrow \infty} \frac{1}{L} \log [\mathcal{L}(t)]. \quad (3)$$

A vanishing value of the return amplitude, and thus of the Loschmidt echo, results in nonanalyticities of the rate function $\lambda(t)$. This is similar to how the complex zeros of partition functions, known as Fisher or Lee-Yang zeros, lead a nonanalytic behavior of the free energy density (i.e. the associated rate function) at the critical point of a phase transition. Extending this idea to the nonequilibrium realm, a DQPT at a critical time t^* (instead of a critical control parameter) is said to occur when during the dynamics, such zeros are crossed [15].

A vast amount of recent theoretical research has been devoted to study this beautiful insight in systems of different nature, namely spin [15, 17–32], fermionic [33–37], bosonic [38–43], and hybrid models [44]. This effort also includes the analysis of the impact of ingredients such as disorder [45, 46] and topological order [47, 48]. Crucially, experimental demonstrations of DQPTs have been achieved in several quantum simulation platforms [49–53]. Many of these studies have shown evidence that DQPTs emerge when there is a quench across an equilibrium quantum phase transition, i.e. when $|\psi_0\rangle$ and the ground state of H correspond to different phases. However, several exceptions have been reported [16, 19, 43], so no one-to-one correspondence between DQPTs and equilibrium quantum phase transitions can be established. In addition, it is common to look for manifestations of dynamical criticality beyond nonanalyticities of $\lambda(t)$. In several cases DQPTs are coincident with vanishing values of order parameters. However, in many others such an association remains elusive [15–18].

To help unravel the connections between DQPTs, equilibrium quantum criticality and the time evolution of observables, it is valuable to consider simple models with different phases that are accessible experimentally. In this regard, systems of strongly interacting spin-1/2 fermions constitute very attractive candidates to be the object of such analysis. In spite of this, DQPTs on these systems have been discussed only a few times [33]. In the present work we perform such a study in the one-dimensional extended Fermi-Hubbard (EFH) model at half filling, which incorporates on-site and nearest-

neighbor density-density interaction. This model not only generalizes the seminal and widely-studied Fermi-Hubbard model, whose dynamics has been intensively explored experimentally with cold atoms in optical lattices [6, 54–57]; it is also known to possess a rich ground-state phase diagram [58–61], and has been recently proposed to explain properties of one-dimensional quantum materials [62, 63]. We analyze DQPTs emerging at early times from quantum quenches in one or both of the interaction terms, with special focus on the Fermi-Hubbard limit and charge density wave (CDW) states. For the former case, we also discuss how symmetries of the model are manifested in the time evolution of the rate function. Furthermore, we establish several cases where a connection to the dynamics of observables can be identified. Finally we show that DQPTs can be induced solely by a time periodic modulation of an on-site potential, which provides a timely strategy for observing such phenomena given the state-of-the-art advances in Floquet engineering with cold fermions in optical lattices [64–67].

The manuscript is organized as follows. In Sec. II we describe the EFH model and the method used to study its dynamics. In Sec. III we show the existence of DQPTs in the Fermi-Hubbard limit ($V = 0$) for noninteracting, weakly and strongly interacting initial states. The transitions resulting from CDW states, namely a ground state of the extended model for finite $V > 0$ and a product degenerate CDW, are discussed in Sec. IV. The emergence of DQPTs from Floquet modulation is presented in Sec. V. Finally, Sec. VI contains our main conclusions.

II. MODEL AND METHOD

We study the DQPTs of the one-dimensional EFH model at half filling, zero magnetization and with open boundary conditions. Its Hamiltonian is given by

$$H = -J \sum_{j=1}^{L-1} \sum_{\sigma=\uparrow,\downarrow} (\hat{c}_{j,\sigma}^\dagger \hat{c}_{j+1,\sigma} + \text{H.c.}) + U \sum_{j=1}^L \hat{n}_{j\uparrow} \hat{n}_{j\downarrow} + V \sum_{j=1}^{L-1} \hat{n}_j \hat{n}_{j+1}, \quad (4)$$

where $\hat{c}_{j,\sigma}^\dagger$ ($\hat{c}_{j,\sigma}$) creates (annihilates) a fermion with spin $\sigma = \uparrow, \downarrow$ on site j , $\hat{n}_{j\sigma} = \hat{c}_{j,\sigma}^\dagger \hat{c}_{j,\sigma}$ is the number operator for site j and spin σ , $\hat{n}_j = \hat{n}_{j\uparrow} + \hat{n}_{j\downarrow}$ is the total number operator at site j , J is the hopping (taken as $J = 1$ to set the energy scale), U the on-site coupling, and V the nearest-neighbor interaction. Thus this model extends the standard (integrable) Fermi-Hubbard Hamiltonian, which corresponds to $V = 0$. Importantly, we allow U and V to represent both repulsive ($U, V > 0$) or attractive ($U, V < 0$) interactions.

The ground state phase diagram of the model at half

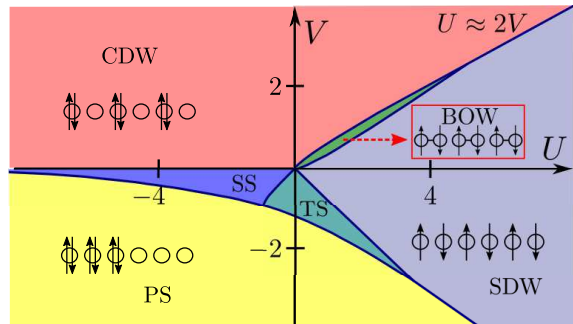


FIG. 1: Qualitative depiction of the ground-state phase diagram of the one-dimensional EFH model at half filling and zero magnetization, adapted from Ref. [61].

filling and zero magnetization, i.e. with

$$\sum_{j=1}^L \langle \hat{n}_{j\uparrow} \rangle = \sum_{j=1}^L \langle \hat{n}_{j\downarrow} \rangle = \frac{L}{2}, \quad (5)$$

is well known [58–61], and features several (quasi-long range ordered) phases, as sketched in Fig. 1. When the system has on-site attraction and nearest-neighbor repulsion, or when the nearest-neighbor repulsion dominates over on-site repulsion, a charge density wave (CDW) is favored. On the other hand, if the on-site repulsion is dominant, a spin density wave (SDW) is formed. For weak and intermediate repulsive interactions, a bond-order wave (BOW) emerges between the CDW and SDW states, characterized by an alternating expectation value of the hopping term of the Hamiltonian [59, 68–74]. For strong nearest-neighbor attraction, the fermions cluster together forming a phase separation (PS). Finally, for weak and intermediate nearest-neighbor attraction, superconducting states are established, either of singlet (SS, with on-site attraction) or triplet (TS) pairing [59, 75].

The dynamical properties of the one-dimensional EFH model are known to a much lesser degree, since most research has focused on the $V = 0$ limit. The latter includes analysis on the expansion of initially-confined particles [56, 76–88], doublon dynamics [89], melting of product ordered states [84, 87, 90, 91], and quantum quenches from ground [84, 92–94] and thermal states [95, 96]. On the other hand, for finite nearest-neighbor interactions, the study on dynamical properties has been much more limited, focusing on the time evolution of doublons [97], time-resolved single-particle spectrum [98], and spectral functions for detecting nonequilibrium superconductivity [99]. Thus the nonequilibrium properties of the EFH model still constitute a largely uncharted territory.

In the present work we discuss the time evolution induced by different sudden quenches in the EFH model, focusing on early times where the existence of DQPTs is unveiled. We consider three main scenarios. First we discuss transitions solely within the Fermi-Hubbard limit. Then we explore quenches from CDW states, cor-

responding to the ground state of the EFH with finite V or a product state. Finally we study DQPTs emerging from a periodic modulation of the Hamiltonian. To reach systems of hundreds of sites, our simulations are based on a matrix product state description. Namely, we calculate the initial state $|\psi_0\rangle$ as the ground state of a Hamiltonian H_0 (with interactions U_0 and V_0) with the density matrix renormalization group [9], and use its time-dependent extension [100, 101] to obtain the evolved state $|\psi_0(t)\rangle$ under Hamiltonian H (with interactions U and V). We show results for chains of $L = 128$ for correlated initial states, and of $L = 256$ for the product CDW (finite-size effects are discussed in Appendix A). We also incorporate the conservation of number of fermions with spin up and down, to work directly in the symmetry sector of half filling and zero magnetization (Eq. (5)). In addition, we take time steps of $\delta t = 0.005$ and bond dimensions up to $\chi = 3000$ during the dynamics. Our codes are based on the open-source Tensor Network Theory library [102, 103].

III. DQPT IN THE FERMI-HUBBARD MODEL

We initiate by discussing DQPTs in the Fermi-Hubbard limit $V_0 = V = 0$. In this case, in addition to the rate function $\lambda(t)$ of Eq. (3), we calculate the average double occupation in the lattice, given by

$$d(t) = \frac{1}{L} \sum_{j=1}^L \langle \hat{n}_{j\uparrow} \hat{n}_{j\downarrow} \rangle(t). \quad (6)$$

We also consider two distinct cases: when the initial state $|\psi_0\rangle$ is noninteracting ($U_0 = 0$) and when it has finite on-site interactions ($U_0 \neq 0$).

A. Initial noninteracting state

We first describe the scenario with $U_0 = 0$, whose results for $L = 128$ are shown in Fig. 2. The cusps featured by the rate function at certain times t_j^* , seen in Fig. 2(a), manifest the emergence of DQPTs for $U \gg 1$, with earlier and more frequent transitions when U increases. In fact, we have verified that the critical time t_1^* of the first DQPT decays essentially as $\sim 1/U$. Also, the differences $\Delta t_j^* = t_{j+1}^* - t_j^*$ between consecutive critical times t_j^* of the transitions shown in Fig. 2(a) are the same for each value of U , and also decay as $\sim 1/U$.

The evolution of the corresponding double occupations is shown in Fig. 2(b), which for short times follows a form

$$d_0 - d(t) \propto \frac{1}{U} \sin^2 \left(\frac{Ut}{2} \right), \quad (7)$$

with $d_0 = 1/4$ the mean double occupation of the noninteracting state at zero magnetization and half filling. Even though the double occupation does not constitute

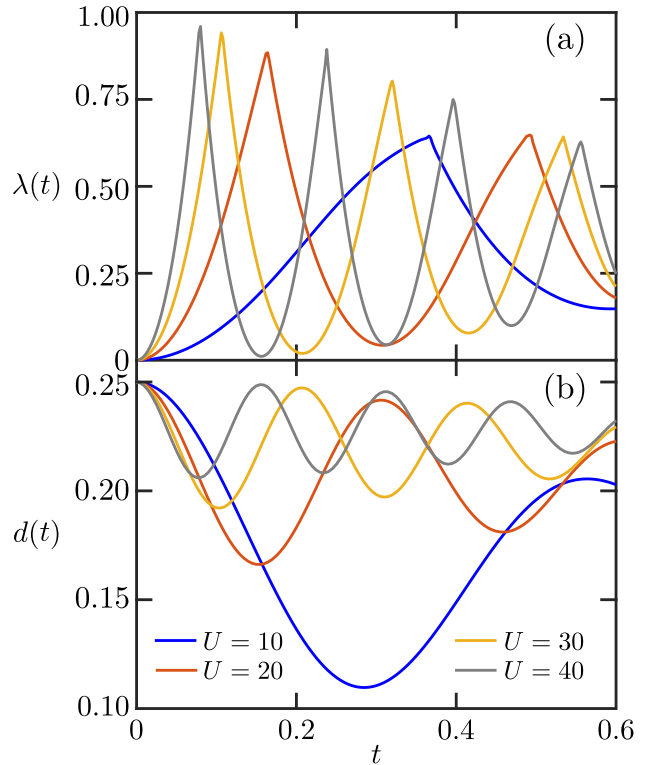


FIG. 2: (a) Rate function $\lambda(t)$ as a function of time for quenches of the Fermi-Hubbard model, with an initial state of $U_0 = 0$. (b) Time evolution of double occupation.

an order parameter of the initial state, the relation between its time evolution and DQPTs is apparent. For $U = 10$ the DQPT occurs somewhat close to the minimum of $d(t)$. For larger values of U the agreement between t_j^* and the times t_j^d of minimal double occupation, given by

$$t_j^d = \frac{\pi}{U} (2j - 1) \quad \text{with } j = 1, 2, \dots \quad (8)$$

according to Eq. (7), becomes better; both times are almost identical for $U = 40$. These results indicate that in this regime of large U and early times, both the DQPTs and charge dynamics are characterized by the same timescale.

We note that for low values of U we did not see DQPTs on early times; for example, for $U = 2$, no DQPT was seen up to the reached time $t = 1.4$. However this does not preclude their appearance much later, which might happen even when the rate function remains smooth for a long time [17].

B. Initial interacting state

Now we discuss the emergence of DQPTs when crossing the metal-insulator transition of the Fermi-Hubbard model at $U = 0$. For this, we prepare initial states $|\psi_0\rangle$

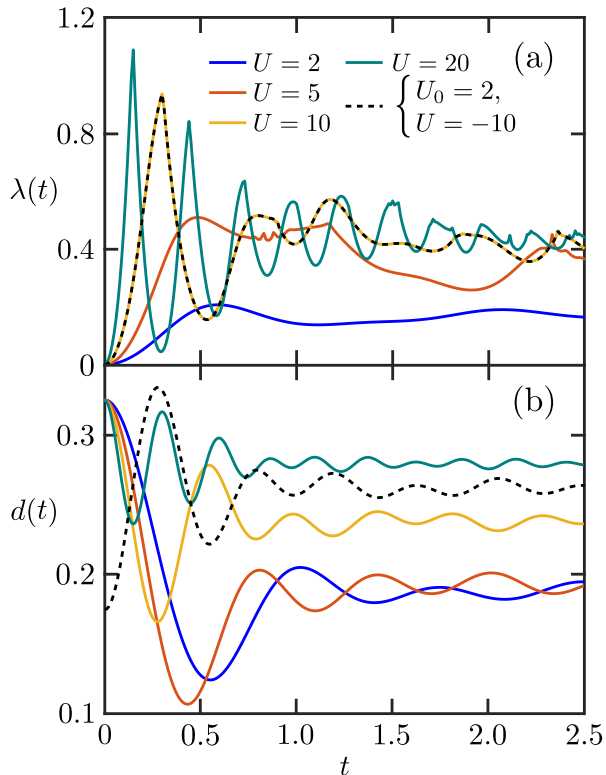


FIG. 3: (a) Rate function $\lambda(t)$ as a function of time for quenches of the Fermi-Hubbard model, with an initial state of $U_0 = -2$. (b) Time evolution of double occupation.

for different finite interactions U_0 and perform the time evolution with values of U at the other side of the transition (no DQPTs were observed when U corresponds to the same equilibrium phase).

We first consider $U_0 = -2$, which corresponds to a metallic state; the rate function for $L = 128$ is shown in Fig. 3(a). For the times considered, $\lambda(t)$ remains smooth for weak repulsive interactions; DQPTs are observed for large enough interactions ($U \gtrsim 5$). For early dynamics and $U \gg 1$, the critical times t_j^* follow a $1/U$ trend, although they are slightly lower than those of $U_0 = 0$. For longer times DQPTs are still observed, but their initial periodicity is lost and their overall profile is different.

The corresponding double occupations are shown in Fig. 3(b), which for large U and early times have a trend similar to Eq. (7) with d_0 the mean double occupation of the initial state. In most cases for strong interactions, local minima of $d(t)$ closely agree with local maxima of the rate function $\lambda(t)$; also, the first maximum of $\lambda(t)$ of $U = 10$, the first three of $U = 20$ and the first five of $U = 30$ (not shown), clearly manifest nonanalytic behavior and thus correspond to DQPTs. For longer times, nonanalyticities of the rate function are also close to minima of $d(t)$, but a one-to-one correspondence is not clear; some do not coincide with a minimum of $d(t)$ (e.g. that of $t = 1.81$ for $U = 20$), some peaks of $\lambda(t)$ do not clearly

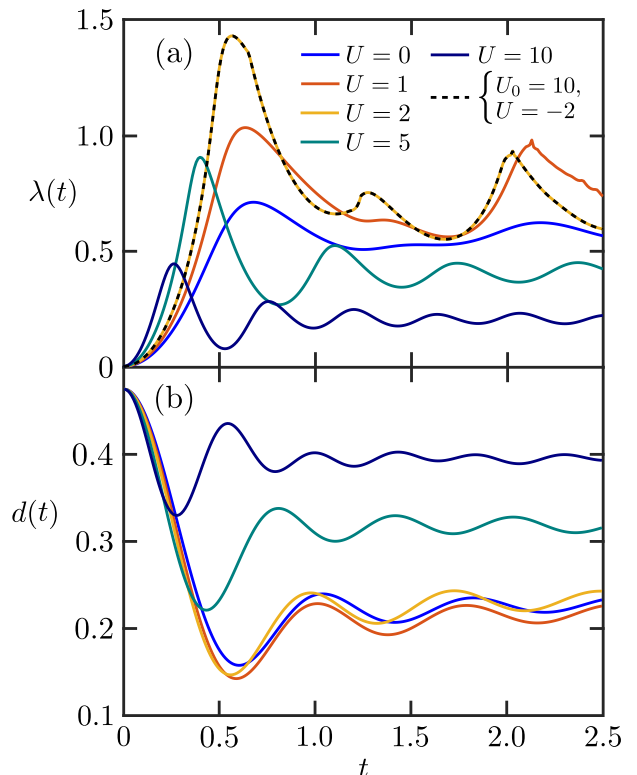


FIG. 4: (a) Rate function $\lambda(t)$ as a function of time for quenches of the Fermi-Hubbard model, with an initial state of $U_0 = -10$. (b) Time evolution of double occupation.

show a nonanalytic behavior (e.g. the first one of $U = 5$, the third and fourth ones of $U = 10$), or the latter is not located at the local maximum (e.g. the second DQPT of $U = 10$). It is possible that simulations with larger system sizes are needed to resolve these fine details. However, at least for early dynamics, the agreement between DQPTs and local minima of $d(t)$ is clear, which spans a longer period of time as U increases.

Now we take an initial state of $U_0 = -10$, also in the metallic phase. As observed in Fig. 4(a), no evidence of DQPTs is found for $U = 0$ or, in contrast to the previous case, for $U \gg 1$. Instead, these take place for weak repulsive interactions. Furthermore, $U = 2$ features the largest number of transitions, with the first two critical times being close to (but not at) the local maxima of $\lambda(t)$; these nonanalyticities are no longer present for the other shown values of U . As seen in Fig. 4(b), the local minima of the mean double occupation occur near the local maxima of $\lambda(t)$, regardless of whether the latter shows a nonanalytic or smooth behavior. Thus a connection between DQPTs and the dynamics of $d(t)$ is not as clear as in the previously discussed scenarios.

An important feature of the time evolution of the Fermi-Hubbard model is evidenced in both Figs. 3 and 4 with a particular example. Namely, the rate function is identical to that obtained when the signs of U_0 and U

are changed (dashed lines). In addition, $d(t)$ is symmetric around the value $1/4$ for this modified time evolution, as depicted in Fig. 3(b). Thus, when the initial state is prepared in the insulating phase and the time evolution is performed under a Hamiltonian with metallic ground state, the correspondence between DQPTs and the mean double occupation takes place for local maxima of the latter. We show these properties in Appendix B, considering the symmetries of the Hamiltonian.

Finally, from the reported results for the reached times, an asymmetry in the directions of the quenches is observed. For example, taking $U_0 = 0$ and $U = 10$ induces a DQPT (Fig. 2) at early times, while considering $U_0 = 10$ and $U = 0$ does not (Fig. 4 and discussion of symmetry of rate function under change of signs).

IV. DQPT FROM CDW STATES

Now we discuss DQPTs from different initial CDW states, namely the ground states of the EFH model for finite (Sec. IV A) and infinite (Sec. IV B) nearest-neighbor attraction V . In addition to $d(t)$, here we calculate the mean imbalance between the population of odd and even sites, given by

$$I(t) = \frac{1}{L} \sum_{j=1}^L (-1)^j \langle \hat{n}_j \rangle. \quad (9)$$

In contrast to cases discussed in Sec. III, here the imbalance shows a sizeable nontrivial dynamical behavior.

A. Finite-coupling CDW

We start by considering DQPTs when the integrability of the Fermi-Hubbard model is broken by including nearest-neighbor interactions $V_0, V \neq 0$. In particular, we consider an initial state with parameters $U_0 = -2$ and $V_0 = 0.5$, which is located in the CDW phase and close to the boundary to the SS (see Fig. 1). The results for $L = 128$ are shown in Fig. 5.

Initially we fixed $V = V_0$ and took several values of $U > 0$, corresponding to quenches into the BOW and SDW states. Similarly to the results in Figs. 2 and 3, for the times reached in the simulations we only found DQPTs for large values of U , deep into the SDW phase. The nonanalyticities of the first few peaks are also similar to the ones reported in those cases. Furthermore, the DQPTs are close to the times of the local minima of the double occupation and get closer as U increases. The local maxima of the imbalance are not as close to the critical times, but their difference Δt^I is quite close to Δt^* for the peaks shown in Fig. 5.

Second, we study a sequence of quenches in a vertical line of the phase diagram of Fig. 1, fixing $U = -2$ and varying V so evolution Hamiltonians with SS and PS ground states are considered. We only found DQPTs

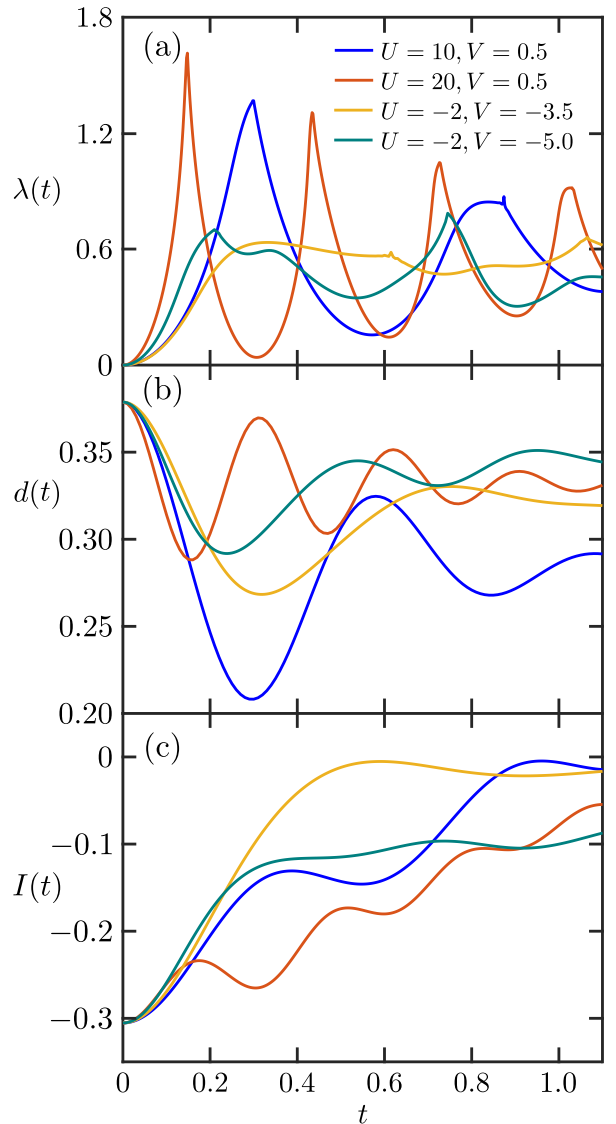


FIG. 5: (a) Rate function $\lambda(t)$ as a function of time for quenches of the Fermi-Hubbard model, with an initial state of $U_0 = -2, V_0 = 0.5$. (b) Time evolution of double occupation. (c) Time evolution of population imbalance. The average of the latter was performed slightly modifying Eq. 9, i.e. we removed 10 sites from each boundary of the chain. In contrast to $d(t)$, the value of the imbalance for this initial state strongly depends on the number of sites removed from the boundaries, although the times of extremal values do not.

after crossing to the PS regime, and show some examples in Fig. 5. When $V = -5$, so one interaction parameter is largely dominant over the other energy scales, the DQPTs are again close to the local minima of $d(t)$ and the maxima of $I(t)$ (only the second DQPT for the latter). For $V = -3.5$ no clear connection between the DQPTs and the dynamics of observables is found.

Finally, we performed quenches varying U and V , to BOW [72, 74] ($U = 2$ and $V = 1, U = 4$ and $V = 2$) and

TS ($U = 0$ and $V = -0.3, -0.5, -0.8$) regimes. For the reached times $t \approx 2$, no DQPTs were observed.

B. Degenerate product CDW

Here we analyze the dynamics of an initial product CDW of the form

$$|\Psi_D^{\uparrow\downarrow,0}\rangle = \prod_{j=1}^{L/2} \hat{c}_{2j-1,\uparrow}^\dagger \hat{c}_{2j,\downarrow}^\dagger |0\rangle = |\uparrow\downarrow \ 0 \ \uparrow\downarrow \ 0 \cdots \uparrow\downarrow \ 0\rangle, \quad (10)$$

where $|0\rangle$ is the vacuum. This state is composed of two sublattices; the one of odd sites is fully occupied and that of even sites is empty. It corresponds to the ground state of an EFH model in the limit $V \rightarrow \infty$ with finite U .

The state of Eq. (10) is degenerate with the product

$$|\Psi_D^{0,\uparrow\downarrow}\rangle = \prod_{j=1}^{L/2} \hat{c}_{2j,\uparrow}^\dagger \hat{c}_{2j,\downarrow}^\dagger |0\rangle = |0 \ \uparrow\downarrow \ 0 \ \uparrow\downarrow \cdots 0 \ \uparrow\downarrow\rangle. \quad (11)$$

To discuss DQPTs arising from degenerate states, an extension to the initial description is necessary. Namely, the full return probability to the ground state manifold is [16, 18]

$$P(t) = \mathcal{L}_{\uparrow\downarrow,0}(t) + \mathcal{L}_{0,\uparrow\downarrow}(t) \quad (12)$$

where $\mathcal{L}_\eta(t) = |\langle \eta | \psi_0(t) \rangle|^2$, and $\eta = \uparrow\downarrow, 0$ and $\eta = 0, \uparrow\downarrow$ denote the two degenerate ground states (10) and (11), respectively. Similarly to the Loschmidt echo (2), each probability $\mathcal{L}_\eta(t) = \exp[-L\lambda_\eta(t)]$ is given by an intensive rate function $\lambda_\eta(t)$. In the thermodynamic limit, one $\mathcal{L}_\eta(t)$ will dominate over the other, so

$$\lambda(t) = - \lim_{L \rightarrow \infty} \frac{1}{L} \log[P(t)] = \min_\eta \lambda_\eta(t). \quad (13)$$

The crossing of the two $\mathcal{L}_\eta(t)$, resulting in a kink, corresponds to a DQPT. This is exemplified in Fig. 6 for $U = 1$ and $V = 0$, where the dashed and line-dotted lines denote the rate functions associated to the two degenerate states. The first two DQPTs result from crossings of the rate functions $\lambda_\eta(t)$, while the third DQPT is a nonanalyticity of the dominating function $\lambda_{\uparrow\downarrow,0}(t)$.

An the crossing point, the ground state symmetry (initially broken by performing the time evolution of state (10)) is restored, which is manifested not only in the return probability $P(t)$ but also in observables; namely a vanishing order parameter at this point is expected. This foretells the importance of the dynamics of the mean imbalance $I(t)$ for the initial state (10).

Given that the initial state we consider here is uncorrelated, we could reach larger system sizes for the quench dynamics than in cases discussed in the other Sections. Thus here we report density matrix renormalization group results for $L = 256$ sites.

1. Fermi-Hubbard limit $V = 0$

First we consider the case $V = 0$ for the time-evolution Hamiltonian. The understanding of these results, shown in Fig. 6, benefits from a key outcome of the symmetries of the Fermi-Hubbard model [90]: the dynamics of the CDW can be directly related to that of the Néel state

$$|\Psi_N\rangle = \prod_{j=1}^{L/2} \hat{c}_{2j-1,\uparrow}^\dagger \hat{c}_{2j,\downarrow}^\dagger |0\rangle = |\uparrow\downarrow \ \uparrow\downarrow \ \uparrow\downarrow \ \cdots \ \uparrow\downarrow\rangle. \quad (14)$$

On the one hand, we show in Appendix C that the Loschmidt echo is equal for both states (10) and (14) when the dynamics is performed under the same Fermi-Hubbard Hamiltonian; we have verified this with our simulations. On the other hand, it has been previously observed that assuming an even number of sites L , both states are related by a symmetry transformation (see Appendix C), and that the expectation values during the time evolution processes are related by [90]

$$d_U^D(t) = d_{-U}^D(t) = \frac{1}{2} - d_U^N(t), \quad (15)$$

$$m_U^N(t) = m_{-U}^N(t) = -I_U^D(t)/2, \quad (16)$$

where the indices D and N indicate the initial CDW and Néel states, respectively, and $m(t)$ is the average staggered magnetization, given by

$$m(t) = \frac{1}{2L} \sum_{j=1}^L (-1)^j \langle \hat{n}_{j\uparrow} - \hat{n}_{j\downarrow} \rangle, \quad (17)$$

which for the CDW melting is zero due to spin inversion symmetry (i.e. there is no direction preference for magnetization alignment). Thus the time evolution of the expectation values of interest is independent of the sign of U , and the known physics of the melting of the one-dimensional Néel state governed by the Fermi-Hubbard model can be directly applied to that of the product CDW [90, 91].

The rate function of Eq. (13) for several values of U is depicted in Fig. 6(a); the mean double occupation and imbalance are shown in Figs. 6(b) and (c), respectively. We start by discussing the $U = 0$ case, given that analytical results for DQPTs and dynamics of observables are known. The former was studied in Ref. [19], formulated in terms of the XXZ model with zero anisotropy (i.e. zero interaction in the spinless-fermion picture) for an initial Néel state. The Fisher zeros $z = R + it$ were shown to be solutions of

$$0 = \int_0^{\pi/2} dk \ln |\tan(z\epsilon_k)|^2, \quad \epsilon_{k_n} = -2J \cos(k_n + a), \quad (18)$$

with $a = \pi/L$, $k_n = 2\pi n/L$, and $n = 0, \dots, L-1$. The real critical times t_j^* correspond to the $R = 0$ solutions, some of which are shown in Table I. The three DQPTs

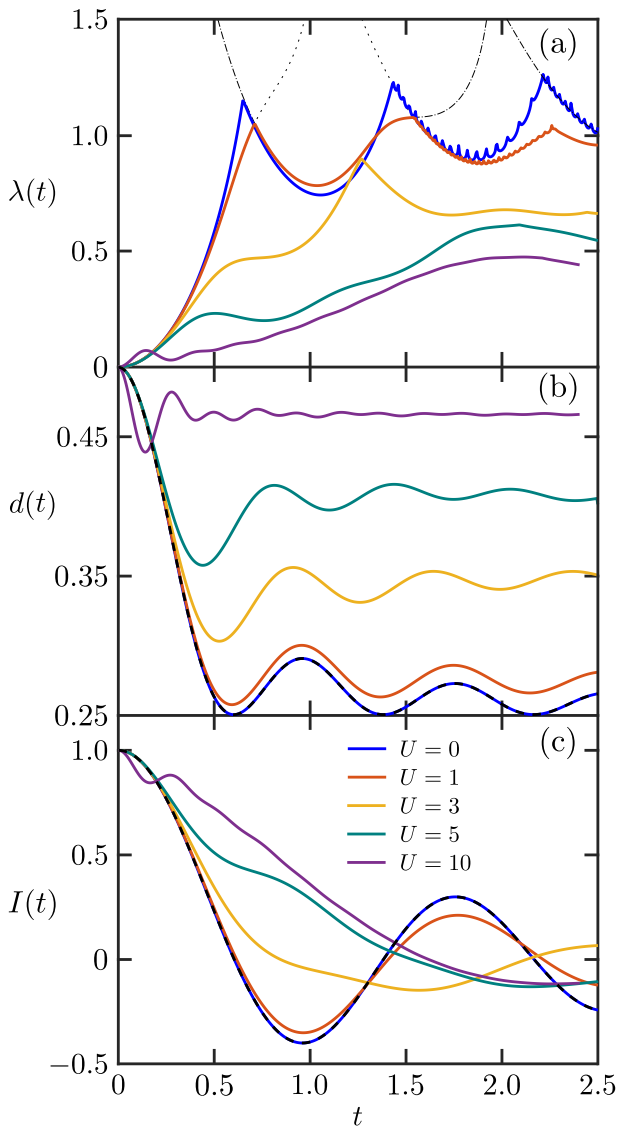


FIG. 6: (a) Rate function $\lambda(t)$ as a function of time for quenches of the Fermi-Hubbard model, with an initial product CDW state of $L = 256$ sites. The dashed and line-dotted lines correspond to the rate functions $\lambda_\eta(t)$ of the two degenerate ground states $\eta = \uparrow\downarrow, 0$ and $\eta = 0, \uparrow\downarrow$, respectively, for $U = 1$. The time scale for the $U = 10$ results has been divided by 2 for better depiction. (b) Time evolution of double occupation. (c) Time evolution of population imbalance. The dashed black lines correspond to the analytical results of Eq. (19) for $U = 0$.

obtained in our simulations ($t_1^* = 0.650, t_2^* = 1.430, t_3^* = 2.215$) occur at the first three times reported in the table. In general, the values of the $U = 0$ rate function shown in Fig. 6(a) agree very well with that of Ref. [19] for the noninteracting XXZ chain [122].

Considering the symmetry restoration argument previously established, we now evaluate whether the times t_j^I of the zeros of the mean charge imbalance $I(t)$, shown in

| j | 1 | 2 | 3 | 4 | 5 | 6 |
|-----------------|-------|-------|-------|-------|-------|-------|
| t_j^* | 0.650 | 1.429 | 2.212 | 2.997 | 3.782 | 4.566 |
| $t_j^I = t_j^d$ | 0.601 | 1.380 | 2.163 | 2.948 | 3.733 | 4.518 |
| $t_j^* - t_j^I$ | 0.049 | 0.049 | 0.049 | 0.049 | 0.049 | 0.048 |

TABLE I: Analytical results of critical times of DQPTs (t_j^*), times of zero imbalance (t_j^I), and their difference, for an initial CDW state and time evolution governed by a noninteracting Fermi-Hubbard Hamiltonian.

Fig. 6(b), correspond to the critical times of the DQPTs. To answer this question, we note that the time evolution of the observables of interest can be obtained exactly in one dimension for $U = 0$, and are given by [90]

$$d(t) = \frac{1 + \mathcal{J}_0^2(4Jt)}{4}, \quad I(t) = \mathcal{J}_0(4Jt), \quad (19)$$

with \mathcal{J}_0 the Bessel function of the first kind. As depicted in Figs. 6(b) and 6(c), our numerical simulations agree very well with these analytical results, and the zeros of the mean imbalance agree with the times t_j^d where the mean double occupation $d(t)$ features the local minimal value $1/4$. In Table I we report the times where these extremal expectation values take place, and see that they are not the same critical times of the DQPTs, but are shifted by a constant factor. Thus, the DQPTs and the time evolution of observables are governed by the same time scales. This is a clear example where both types of quantities are directly related.

Now we discuss the impact of turning the local interaction $U > 0$ on. We emphasize two important points here. First, there are DQPTs for any U . This might be unexpected for large interactions because they correspond to a Hamiltonian deep in the SDW phase (see Fig. 1), and as previously stated, the rate function is identical to that emerging from the Néel state. However we will argue that this is indeed the case. Second, as in the noninteracting limit, the dynamics of the imbalance and double occupation can be extracted from those of the magnetization and double occupation for an initial Néel state, which have been previously studied [90, 91].

We initially consider weak interactions. For finite $U/J \lesssim 1$, both $d(t)$ and $I(t)$ have a similar behavior to those of the noninteracting case; the dynamics is highly-oscillating and rapidly tends to the steady-state values [91]. As shown in Fig. 6(a) for $U = 1$, $\lambda(t)$ is also close to that of $U = 0$. However, qualitative differences in the dynamics start to emerge. First, the zeros of the charge imbalance no longer agree with the double occupation minima (even though they remain close). More importantly, the connection between DQPTs and observables becomes less clear. Compared to the results in Table I, the first zero of the imbalance moves to a slightly higher value ($t_1^I \approx 0.615$) while the first critical time increases more ($t_1^* \approx 0.710$); also, the subtractions of consecutive times Δt_j^* , Δt_j^d and Δt_j^I do not agree anymore. When

the system has stronger interactions these differences are accentuated, as already evident for $U = 3$.

The dynamics of expectation values for even stronger interactions $U/J \gg 1$ has also been previously analyzed. Here different types of evolutions are seen. Namely, for short times $Jt \lesssim 0.5$, second-order time-dependent perturbation theory can be used to characterize the rapidly-decaying oscillations [91]:

$$\begin{aligned} d(t) &= \frac{1}{2} - \frac{8J^2}{U^2} \sin^2\left(\frac{Ut}{2}\right), \\ I(t) &= 1 - \frac{16J^2}{U^2} \sin^2\left(\frac{Ut}{2}\right). \end{aligned} \quad (20)$$

For long times the relaxation of the imbalance is slower than that of the double occupation, where the former is governed by the effective exchange interaction $J_{\text{ex}} = 4J^2/U$. Furthermore, $d(t)$ relaxes showing very small oscillations with frequency U around its steady-state value, while $I(t)$ features wide oscillations with frequency $\propto J_{\text{ex}}$ [91]. The results shown in Figs. 6(b) and 6(c) for $U = 5, 10$ agree with this description. Regarding $\lambda(t)$, depicted in Fig. 6(a), its first critical time t_1^* increases with U ; for example, that of $U = 10$ is $t_1^* = 4.42$. Also, the corresponding nonanalytic behavior of the rate function, resulting from the crossing of both $\lambda_\eta(t)$, becomes less sharp. In addition, the relation of observables to DQPTs is blurred even further, since no correspondence to particular characteristics of $d(t)$ or $I(t)$ is found.

In the limit of very large U/J the melting of the CDW state is essentially described by the Heisenberg model

$$H_{\text{Heis}} = J_{\text{ex}} \sum_i \vec{S}_i \cdot \vec{S}_{i+1}, \quad (21)$$

which is derived from the Fermi-Hubbard model by a Schrieffer-Wolf transformation [91, 104]. Thus, the double occupation of the evolving CDW is $d(t) \approx 1/2$ (equivalent to impeded double occupation in the Néel state dynamics, see Eq. (15)), and the long-time evolution of its charge imbalance is entirely governed by J_{ex} . Regarding the rate function, we note that a DQPT with an initial Néel state and the time evolution governed by the Heisenberg model (21) has been reported, where a relation to the energy-resolved order parameter was found [18]. Thus this limit should be recovered when starting from a product CDW and evolving with a very large U for a time longer than $t_1^* \sim 1/U$. For the largest U considered here ($U = 20, 30$), the time reached in our simulations was not enough to capture the transition.

2. Finite nearest-neighbor interaction $V \neq 0$

When setting $V > 0$ the dynamics becomes more involved, as another energy scale comes into play. Furthermore, the symmetry discussed in Appendix C is no longer valid, as the unitary transformation encoding it leads

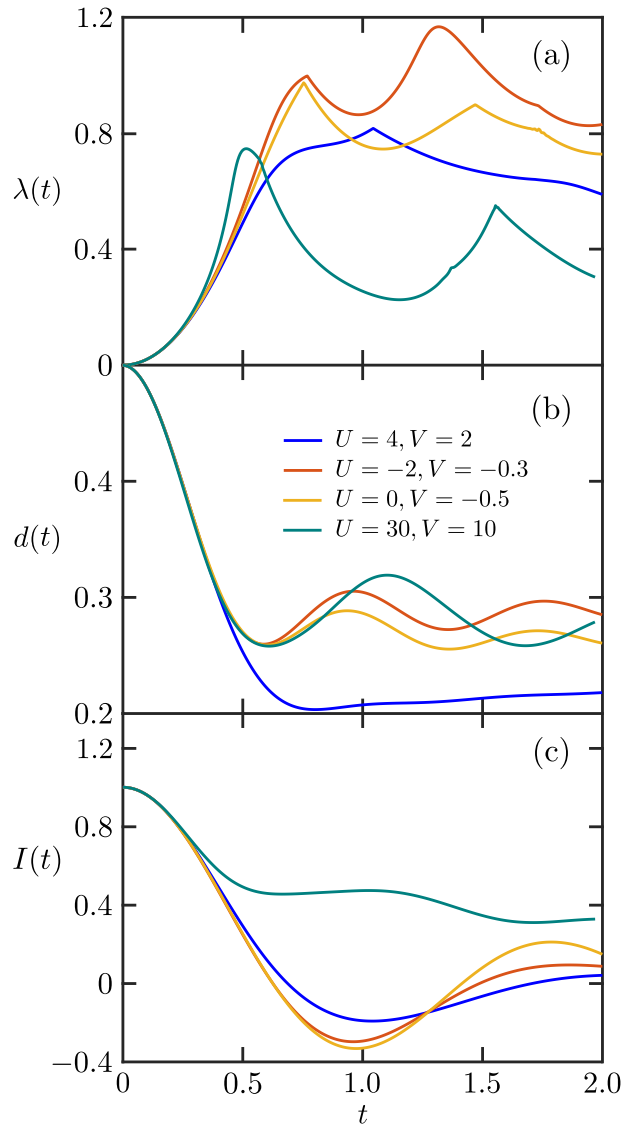


FIG. 7: (a) Rate function $\lambda(t)$ as a function of time for quenches of the extended Fermi-Hubbard model, with an initial product CDW state of $L = 256$ sites. (b) Time evolution of double occupation. (c) Time evolution of population imbalance.

to a spin-type $\hat{S}_i^z \hat{S}_{i+1}^z$ term when acting on the nearest-neighbor interaction of the Hamiltonian [90]. Thus the results for an initial Néel state are different to those of the product CDW.

We simulated the dynamics in this case for quenches from the product CDW to Hamiltonians corresponding to several different phases, for systems of $L = 256$. Figure 7(a) shows some examples of rate functions that feature DQPTs; note that these emerge on early times for cases in which no nonanalyticities were observed for the finite-coupling CDW initial state of Sec. IV A. Figures 7(b) and 7(c) present the corresponding mean double occupation and population imbalance.

For quenches taking Hamiltonians with superconducting ground states ($U = -2$ and $V = -0.3$ for SS, $U = 0$ and $V = -0.5$ for TS), the double occupation and the population imbalance are highly oscillating in time, being similar to that of the noninteracting case. On the other hand, the location of DQPTs is not evidently related to that of the zeros of $I(t)$ or the local minima of $d(t)$; the same can be said for the very-different time separation between consecutive cusps.

For a quench Hamiltonian with stronger interactions and BOW ground state ($U = 4$, $V = 2$), where the oscillations of the observables are heavily damped, the observed DQPT is very close to the minimal imbalance (both at time ≈ 1.040). Finally, for an extreme SDW case ($U = 30$ and $V = 10$), where the charge imbalance approaches its steady state value on a larger time scale than the double occupation, the clear DQPTs do not coincide with any notable behavior of the observables.

V. DQPT INDUCED BY PERIODIC DRIVING

Finally, we discuss an alternative and far less explored method to induce DQPTs. This corresponds to driving the system by an external periodic excitation [50, 105–109], where the average dynamics can be described by an effective (Floquet) Hamiltonian. To perform this study, we first calculate the ground state of the EFH model at half filling for particular values of U_0 and V_0 . Then we perform a real time evolution with $U = U_0$, $V = V_0$, and a time-periodic electric field of the form

$$H_{\text{driv}} = E \sum_j j \sin(\omega t) \hat{n}_j, \quad (22)$$

with frequency ω . Moving to a rotating frame, the time-periodic electric field is transformed into a time-dependent hopping parameter given by

$$J(t) = J e^{iA \cos(\omega t)}, \quad \text{with } A = E/\omega. \quad (23)$$

Thus the hopping is multiplied by a Peierls phase. In this way, the emerging DQPTs are a direct consequence of the driving protocol, which is controlled by the frequency ω and the amplitude A .

To discuss these Floquet DQPTs, we focus on a high-frequency driving ($\omega = 15$ and $A = 3$), which is known to correspond to an effective Hamiltonian in which the hopping is renormalized by the Bessel function $\mathcal{J}_0(A)$ [110–112]; this is equivalent to having new density-density interactions $U/\mathcal{J}_0(A)$ and $V/\mathcal{J}_0(A)$. The results are shown in Fig. 8 for two initial states in different phases, namely an insulating SDW state for the Fermi-Hubbard Hamiltonian and a CDW for the extended model; we see in both cases that the evolution of the double occupation and the rate function is very well captured, in average, by that of the effective Hamiltonian.

For a SDW initial state with $U_0 = 2$ and $V_0 = 0$ the effective Floquet Hamiltonian has $U = -2/\mathcal{J}_0(3) \approx -7.69$

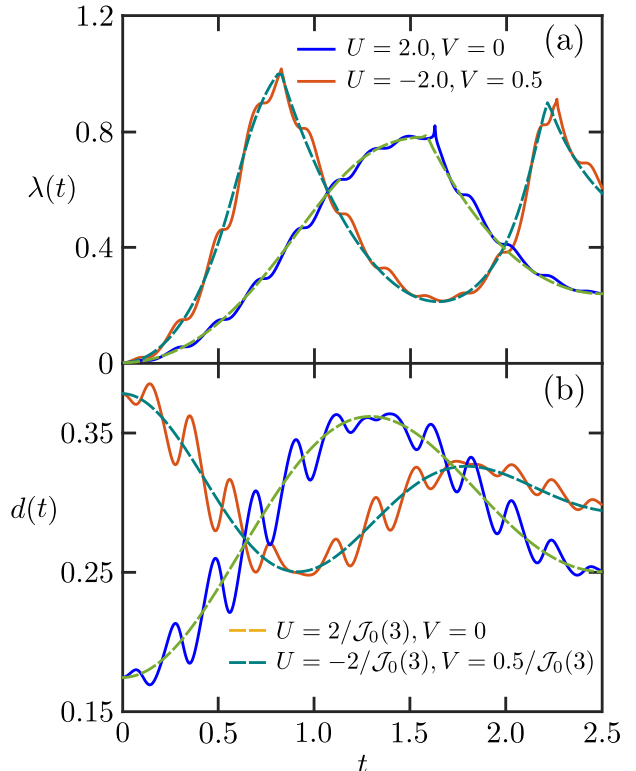


FIG. 8: DQPTs induced by periodic high-frequency driving, with $\omega = 15$ and $A = 3$. (a) Rate function $\lambda(t)$ as a function of time. (b) Time evolution of double occupation $d(t)$. The solid lines correspond to the results for the driven systems, and the dashed lines to those of the lattices with effective Floquet Hamiltonian.

and $V = 0$, which corresponds to a metallic ground state; considering the results of Sec. III B, a DQPT is expected, and indeed observed in Fig. 8(a). A similar result is obtained for a CDW case with $U_0 = -2$ and $V_0 = 0.5$, since the effective Hamiltonian corresponds to $U = 2/\mathcal{J}_0(3) \approx 7.69$ and $V = 0.5/\mathcal{J}_0(3) \approx -1.92$, which has a ground state deep in the SDW regime. In the light of the results of Sec. IV A, DQPTs are expected and observed, as depicted in Fig. 8(a).

Our results thus show that the form and time of occurrence of DQPTs can be controlled with a periodic external field, by the amplitude of the driving. In addition to the existing capabilities for implementing Fermi-Hubbard models in cold-atom architectures [6, 54–57], recent advances in simulating periodic driving of the form (22) by mechanical shaking [64–67] make our proposal a very-promising scheme for observing DQPTs in experiments.

VI. CONCLUSIONS

The rich ground state phase diagram of systems of interacting fermions makes them an ideal testbed for observing DQPTs and establishing connections to singu-

lar characteristics of observables. With this in mind, we performed an analysis of DQPTs in the one-dimensional EFH model at half filling, for several interaction regimes.

We initially considered the standard Fermi-Hubbard Hamiltonian ($V_0 = V = 0$). For a noninteracting initial state ($U_0 = 0$), transitions are found for strong interactions $U > 0$, and agree with local minima of the double occupation. A one-to-one correspondence between both becomes less clear for a weakly-attractive initial state ($U_0 = -2$), and blurs even further for a stronger-interacting case ($U_0 = -10$), for which DQPTs are only seen for weak $U > 0$. Notably, the same dynamics of the rate function emerges when the signs of the ground-state and time-evolution Hamiltonians are changed.

Subsequently we analyzed DQPTs within the extended model ($V \neq 0$) from initial CDWs. When starting from a state with weak nearest-neighbor repulsion ($V_0 = 0.5$), transitions were found for time-evolving Hamiltonians deep into the SDW and PS regimes. A connection between nonanalyticities of the rate function and special characteristics of observables seems to emerge when one interaction is largely dominant. A different correspondence is seen for some DQPTs when starting from a product CDW. This is particularly transparent for an evolution governed by a noninteracting Hamiltonian, for both the population imbalance and the mean double occupation. In addition, DQPTs are observed here even for quenches in which the first CDW did not feature them, namely to BOW, SS and TS regimes.

Finally, we demonstrated the emergence of DQPTs solely from a time-periodic on-site potential. Performing a high-frequency modulation on initial insulating SDW and CDW states, DQPTs were induced and captured by an evolution with an effective Floquet Hamiltonian.

Our results suggest a new platform to observe experimentally a wide variety of DQPTs. On the one hand, protocols for obtaining the Loschmidt echo in ultracold atom setups have been proposed [113–115]. Also, it has already been possible to create a product CDW in fermionic optical lattice setups [55]. Furthermore, the existing capabilities to implement time-periodic Hamiltonians [64–67] makes the observation of DQPTs resulting from Floquet engineering very promising. Even though state-of-the-art cold-atom quantum simulators have been created for the Fermi-Hubbard model ($V = 0$) [57], future developments of the extended model might be motivated by our work.

On the theoretical side, our work motivates the search of DQPTs from different phases, e.g. superconducting or BOW states, and of a connection to the dynamics of their order parameters. Furthermore, it inspires the analysis of more complex systems with rich phase diagrams such as Bose-Fermi mixtures, which have been implemented in cold atom setups [116–118] and whose dynamics can be simulated efficiently with tensor networks [119, 120]. Finally, different driving schemes could be exploited, e.g. resonant driving, whose effective Hamiltonian, being quite different to the Fermi-Hubbard model [121], seems appealing to induce DQPTs.

Acknowledgments

The author acknowledges discussions with L. Quiroga and F. Rodríguez, and is thankful to S.R. Clark for his comments on the manuscript. The author also thanks the support of Banco de la República, through project No. 4.392: *Control de ondas de densidad de carga y superconductividad en sistemas fermiónicos por medio de forzamiento periódico*, and of UK's Engineering and Physical Sciences Research Council (EPSRC) under grant EP/T028424/1. This work was carried out using the computational facilities of the Advanced Computing Research Centre, University of Bristol - <http://www.bristol.ac.uk/acrc/>, and of Universidad de los Andes High Performance Computing (HPC) Centre.

Appendix A: Finite-size effects on DQPTs

As discussed in the main text, DQPTs are defined in the thermodynamic limit. In our simulations we have access to finite systems only; however we see that as the system size L increases, the sharp features that signal the emergence of such transitions develop. This is exemplified in Fig. 9(a) for the first peak of the rate function corresponding to an initial finite- V CDW; a similar trend is observed in other cases. We also present results of different sizes for a transition emerging from the product CDW in Fig. 9(b), where a sharp behavior is already seen for small systems due to the crossing of the rate functions λ_η for both η . These results thus point towards nonanalytic features in the thermodynamic limit. We note that away from these, $\lambda(t)$ is essentially independent of the values of L considered.

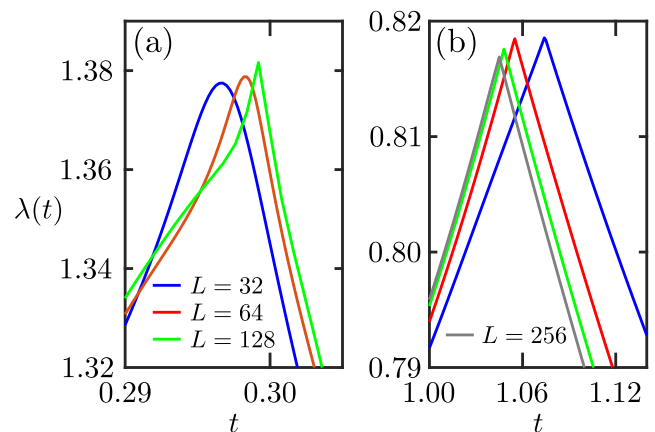


FIG. 9: Rate function $\lambda(t)$ as a function of time for different scenarios and system sizes. (a) $U_0 = -2$, $V_0 = 0.5$, $U = 10$ and $V = 0.5$ (see Fig. 5). (b) Initial CDW state, $U = 4$ and $V = 2$ (see Fig. 7). The time step was reduced up to $\delta t = 2 \times 10^{-4}$ to better describe the peak.

Appendix B: DQPT symmetry of Fermi-Hubbard model under signs exchange

Here we demonstrate the symmetry of the rate function when the signs of the on-site density-density interactions are changed. For this we consider the ground state Hamiltonians \hat{H}_+^g and \hat{H}_-^g , with couplings $+U_0$ and $-U_0$ respectively, and the time evolution Hamiltonians \hat{H}_+^e and \hat{H}_-^e , with couplings $+U$ and $-U$ respectively. As discussed in Ref. [90], the unitary transformation

$$\hat{U} = \prod_j \left(\hat{c}_{j\uparrow} + (-1)^j \hat{c}_{j\uparrow}^\dagger \right) \quad (\text{B1})$$

relates the attractive and repulsive Fermi-Hubbard models. Thus it is easily shown that

$$\hat{U}^\dagger \hat{H}_+^g \hat{U} = \hat{H}_-^g, \quad \hat{U}^\dagger \hat{H}_+^e \hat{U} = \hat{H}_-^e, \quad (\text{B2})$$

and vice versa. Thus, for any time t ,

$$\hat{U}^\dagger \exp(-it\hat{H}_-^e) \hat{U} = \exp(-it\hat{H}_+^e). \quad (\text{B3})$$

Condition (B2) also leads to the relation between the ground states of the respective Hamiltonians

$$\hat{U}^\dagger |\psi_+^g\rangle = |\psi_-^g\rangle. \quad (\text{B4})$$

One form to show this result consists of taking the ground state as the infinite-time limit of an imaginary time evolution [100], namely

$$|\psi_+^g\rangle = \lim_{\tau \rightarrow \infty} \frac{\exp(-\tau\hat{H}_+^g) |\phi\rangle}{\|\exp(-\tau\hat{H}_+^g) |\phi\rangle\|}, \quad (\text{B5})$$

for some initial state $|\phi\rangle$ which has a nonzero overlap with $|\psi_+^g\rangle$. Thus we get

$$\begin{aligned} \hat{U}^\dagger |\psi_+^g\rangle &= \lim_{\tau \rightarrow \infty} \frac{\hat{U}^\dagger \exp(-\tau\hat{H}_+^g) |\phi\rangle}{\langle \phi | \exp(-\tau\hat{H}_+^g) \exp(-\tau\hat{H}_+^g) |\phi\rangle^{1/2}} \\ &= \lim_{\tau \rightarrow \infty} \frac{\exp(-\tau\hat{H}_-^g) \hat{U}^\dagger |\phi\rangle}{\langle \phi | \hat{U} \exp(-\tau\hat{H}_-^g) \exp(-\tau\hat{H}_-^g) \hat{U}^\dagger |\phi\rangle^{1/2}} \\ &= \lim_{\tau \rightarrow \infty} \frac{\exp(-\tau\hat{H}_-^g) \hat{U}^\dagger |\phi\rangle}{\|\exp(-\tau\hat{H}_-^g) \hat{U}^\dagger |\phi\rangle\|} = |\psi_-^g\rangle, \end{aligned} \quad (\text{B6})$$

provided $\hat{U}^\dagger |\phi\rangle$ has a nonzero overlap with $|\psi_-^g\rangle$. Using Eqs. (B3) and (B4) we have, for the Loschmidt amplitude of the dynamics with initial state $|\psi_+^g\rangle$ and time evolution under \hat{H}_-^e

$$\begin{aligned} \langle \psi_+^g | \exp(-it\hat{H}_-^e) | \psi_+^g \rangle &= \langle \psi_+^g | \hat{U} \hat{U}^\dagger \exp(-it\hat{H}_-^e) \hat{U} \hat{U}^\dagger | \psi_+^g \rangle \\ &= \langle \psi_-^g | \exp(-it\hat{H}_+^e) | \psi_-^g \rangle. \end{aligned} \quad (\text{B7})$$

The Loschmidt amplitude, and thus the echo and the rate function, are invariant under the change of signs of the on-site interactions of the ground state and time evolution Hamiltonians.

Similarly, the time evolution of the double occupation $\hat{d}_j = \hat{n}_{j\uparrow} \hat{n}_{j\downarrow}$ of site j under the same scheme as in Eq. (B7), which we name $d_j^{+-}(t)$ (first sign in the exponent indicating $+U$ for ground state, and second sign indicating $-U$ for time evolution), is given by

$$\begin{aligned} d_j^{+-}(t) &= \langle \psi_+^g | \exp(it\hat{H}_-^e) \hat{d}_j \exp(-it\hat{H}_-^e) | \psi_+^g \rangle = \\ &= \langle \psi_+^g | \hat{U} \hat{U}^\dagger \exp(it\hat{H}_-^e) \hat{U} \hat{U}^\dagger \hat{d}_j \hat{U} \hat{U}^\dagger \exp(-it\hat{H}_-^e) \hat{U} \hat{U}^\dagger | \psi_+^g \rangle = \\ &= \langle \psi_-^g | \exp(it\hat{H}_+^e) (\hat{n}_{j\downarrow} - \hat{d}_j) \exp(-it\hat{H}_+^e) | \psi_-^g \rangle, \end{aligned} \quad (\text{B8})$$

where in the last equality we used that $\hat{U}^\dagger \hat{d}_j \hat{U} = \hat{n}_{j\downarrow} - \hat{d}_j$. Performing an average of the terms of Eq. (B8) over all sites j , and considering that the number on fermions with spin down is a constant of motion with value given by Eq. (5), we finally get

$$d_j^{+-}(t) \equiv \frac{1}{L} \sum_{j=1}^L d_j^{+-}(t) = \frac{1}{2} - \sum_{j=1}^L d_j^{-+}(t) \equiv \frac{1}{2} - d_j^{+-}(t). \quad (\text{B9})$$

Thus the average double occupations for the evolution schemes with exchanged interaction signs are symmetric with respect to 1/4.

Appendix C: Symmetry between dynamics of CDW and Néel states

In Ref. [90] it was shown that the product CDW and Néel states are related through the unitary (B1) by

$$|\Psi_N\rangle = \hat{U}^\dagger |\Psi_D\rangle, \quad |\Psi_D\rangle = \hat{U} |\Psi_N\rangle. \quad (\text{C1})$$

Furthermore, based on the unitary transformation and on the time reversal invariance of the expectation values, Eqs. (16) and (15) were demonstrated. Now we show that the Loschmidt echoes, and thus the rate function, is equal when a quench is performed on both states with the same Fermi-Hubbard Hamiltonian (the Loschmidt amplitudes themselves might be different, as observed from our simulations). Starting from the echo for a Néel state:

$$\begin{aligned} &|\langle \Psi_N | \exp(-it\hat{H}^e) | \Psi_N \rangle|^2 = \\ &\langle \Psi_N | \exp(-it\hat{H}^e) | \Psi_N \rangle \langle \Psi_N | \exp(it\hat{H}^e) | \Psi_N \rangle = \\ &\langle \Psi_D | \hat{U} \exp(-it\hat{H}^e) \hat{U}^\dagger | \Psi_D \rangle \langle \Psi_D | \hat{U} \exp(it\hat{H}^e) \hat{U}^\dagger | \Psi_D \rangle = \\ &|\langle \Psi_D | \exp(-it\hat{H}^e) | \Psi_D \rangle|^2, \end{aligned} \quad (\text{C2})$$

thus obtaining the echo for the product CDW.

-
- [1] M. Rigol, V. Dunjko, and M. Olshanii, *Nature* **452**, 854 (2008).
- [2] R. Nandkishore and D. A. Huse, *Annual Review of Condensed Matter Physics* **6**, 15 (2015).
- [3] J. Eisert, M. Friesdorf, and C. Gogolin, *Nat. Phys.* **11**, 124 (2015).
- [4] A. M. Kaufman, M. E. Tai, A. Lukin, M. Rispoli, R. Schittko, P. M. Preiss, and M. Greiner, *Science* **353**, 794 (2016), ISSN 0036-8075.
- [5] M. Ueda, *Nat. Rev. Phys.* **2**, 669 (2020).
- [6] U. Schneider, L. Hackermüller, J. P. Ronzheimer, S. Will, S. Braun, T. Best, I. Bloch, E. Demler, S. Mandt, D. Rasch, et al., *Nat. Phys.* **8**, 213 (2012).
- [7] P. N. Jepsen, J. Amato-Grill, I. Dimitrova, W. W. Ho, E. Demler, and W. Ketterle, *Nature* **588**, 403 (2020).
- [8] B. Bertini, F. Heidrich-Meisner, C. Karrasch, T. Prosen, R. Steinigeweg, and M. Žnidarič, *Rev. Mod. Phys.* **93**, 025003 (2021).
- [9] U. Schollwöck, *Ann. Phys.* **326**, 96 (2011).
- [10] H. Aoki, N. Tsuji, M. Eckstein, M. Kollar, T. Oka, and P. Werner, *Rev. Mod. Phys.* **86**, 779 (2014).
- [11] R. Orús, *Nat. Rev. Phys.* **1**, 538 (2019).
- [12] I. M. Georgescu, S. Ashhab, and F. Nori, *Rev. Mod. Phys.* **86**, 153 (2014).
- [13] F. Schäfer, T. Fukuhara, S. Sugawa, Y. Takasu, and Y. Takahashi, *Nat. Rev. Phys.* **2**, 411 (2020).
- [14] E. Altman, K. R. Brown, G. Carleo, L. D. Carr, E. Demler, C. Chin, B. DeMarco, S. E. Economou, M. A. Eriksson, K.-M. C. Fu, et al., *PRX Quantum* **2**, 017003 (2021).
- [15] M. Heyl, A. Polkovnikov, and S. Kehrein, *Phys. Rev. Lett.* **110**, 135704 (2013).
- [16] M. Heyl, *Rep. Prog. Phys.* **81**, 054001 (2018).
- [17] C. Karrasch and D. Schuricht, *Phys. Rev. B* **87**, 195104 (2013).
- [18] M. Heyl, *Phys. Rev. Lett.* **113**, 205701 (2014).
- [19] F. Andraschko and J. Sirker, *Phys. Rev. B* **89**, 125120 (2014).
- [20] S. Vajna and B. Dóra, *Phys. Rev. B* **89**, 161105 (2014).
- [21] M. Heyl, *Phys. Rev. Lett.* **115**, 140602 (2015).
- [22] M. Schmitt and S. Kehrein, *Phys. Rev. B* **92**, 075114 (2015).
- [23] U. Divakaran, S. Sharma, and A. Dutta, *Phys. Rev. E* **93**, 052133 (2016).
- [24] J. C. Halimeh and V. Zauner-Stauber, *Phys. Rev. B* **96**, 134427 (2017).
- [25] I. Homrighausen, N. O. Abeling, V. Zauner-Stauber, and J. C. Halimeh, *Phys. Rev. B* **96**, 104436 (2017).
- [26] B. Žunkovič, M. Heyl, M. Knap, and A. Silva, *Phys. Rev. Lett.* **120**, 130601 (2018).
- [27] D. M. Kennes, D. Schuricht, and C. Karrasch, *Phys. Rev. B* **97**, 184302 (2018).
- [28] G. Sun and B.-B. Wei, *Phys. Rev. B* **102**, 094302 (2020).
- [29] S. Haldar, S. Roy, T. Chanda, A. Sen(De), and U. Sen, *Phys. Rev. B* **101**, 224304 (2020).
- [30] J. C. Halimeh, M. Van Damme, V. Zauner-Stauber, and L. Vanderstraeten, *Phys. Rev. Research* **2**, 033111 (2020).
- [31] C. Ding, *Phys. Rev. B* **102**, 060409 (2020).
- [32] S. De Nicola, A. A. Michailidis, and M. Serbyn, *Phys. Rev. Lett.* **126**, 040602 (2021).
- [33] E. Canovi, P. Werner, and M. Eckstein, *Phys. Rev. Lett.* **113**, 265702 (2014).
- [34] L. Pastori, S. Barbarino, and J. C. Budich, *Phys. Rev. Research* **2**, 033259 (2020).
- [35] P. Uhrich, N. Defenu, R. Jafari, and J. C. Halimeh, *Phys. Rev. B* **101**, 245148 (2020).
- [36] C. Rylands and V. Galitski, arXiv:2001.10084v2 (2020).
- [37] C. Rylands, E. A. Yuzbashyan, V. Gurarie, A. Zabalo, and V. Galitski, arXiv:2103.03754 (2021).
- [38] T. Fogarty, A. Usui, T. Busch, A. Silva, and J. Goold, *New J. Phys.* **19**, 113018 (2017).
- [39] M. Lacki and M. Heyl, *Phys. Rev. B* **99**, 121107 (2019).
- [40] M. Abdi, *Phys. Rev. B* **100**, 184310 (2019).
- [41] R. Liao, F. Xiong, and X. Chen, *Phys. Rev. A* **103**, 043312 (2021).
- [42] M. Syed, T. Enss, and N. Defenu, *Phys. Rev. B* **103**, 064306 (2021).
- [43] S. Stumper, M. Thoss, and J. Okamoto, arXiv:2106.10187 (2021).
- [44] R. Puebla, *Phys. Rev. B* **102**, 220302 (2020).
- [45] H. Yin, S. Chen, X. Gao, and P. Wang, *Phys. Rev. A* **97**, 033624 (2018).
- [46] K. Cao, W. Li, M. Zhong, and P. Tong, *Phys. Rev. B* **102**, 014207 (2020).
- [47] M. Heyl and J. C. Budich, *Phys. Rev. B* **96**, 180304 (2017).
- [48] I. Hagymási, C. Hubig, O. Legeza, and U. Schollwöck, *Phys. Rev. Lett.* **122**, 250601 (2019).
- [49] P. Jurcevic, H. Shen, P. Hauke, C. Maier, T. Brydges, C. Hempel, B. P. Lanyon, M. Heyl, R. Blatt, and C. F. Roos, *Phys. Rev. Lett.* **119**, 080501 (2017).
- [50] N. Fläschner, D. Vogel, M. Tarnowski, B. S. Rem, D.-S. Lühmann, M. Heyl, J. C. Budich, L. Mathey, K. Sengstock, and C. Weitenberg, *Nat. Phys.* **14**, 265 (2018).
- [51] X.-Y. Guo, C. Yang, Y. Zeng, Y. Peng, H.-K. Li, H. Deng, Y.-R. Jin, S. Chen, D. Zheng, and H. Fan, *Phys. Rev. Applied* **11**, 044080 (2019).
- [52] K. Wang, X. Qiu, L. Xiao, X. Zhan, Z. Bian, W. Yi, and P. Xue, *Phys. Rev. Lett.* **122**, 020501 (2019).
- [53] X. Nie, B.-B. Wei, X. Chen, Z. Zhang, X. Zhao, C. Qiu, Y. Tian, Y. Ji, T. Xin, D. Lu, et al., *Phys. Rev. Lett.* **124**, 250601 (2020).
- [54] J. P. Ronzheimer, M. Schreiber, S. Braun, S. S. Hodgman, S. Langer, I. P. McCulloch, F. Heidrich-Meisner, I. Bloch, and U. Schneider, *Phys. Rev. Lett.* **110**, 205301 (2013).
- [55] M. Schreiber, S. S. Hodgman, P. Bordia, H. P. Lüschen, M. H. Fischer, R. Vosk, E. Altman, U. Schneider, and I. Bloch, *Science* **349**, 842 (2015).
- [56] S. Scherg, T. Kohlert, J. Herbrych, J. Stolpp, P. Bordia, U. Schneider, F. Heidrich-Meisner, I. Bloch, and M. Aidelsburger, *Phys. Rev. Lett.* **121**, 130402 (2018).
- [57] L. Tarruell and L. Sanchez-Palencia, *C. R. Physique* **9**, 365 (2018).
- [58] R. T. Clay, A. W. Sandvik, and D. K. Campbell, *Phys. Rev. B* **59**, 4665 (1999).
- [59] M. Nakamura, *Phys. Rev. B* **61**, 16377 (2000).
- [60] S.-S. Deng, S.-J. Gu, and H.-Q. Lin, *Phys. Rev. B* **74**, 045103 (2006).
- [61] F. Iemini, T. O. Maciel, and R. O. Vianna, *Phys. Rev. B* **92**, 075423 (2015).

- [62] Z. Chen, Y. Wang, S. N. Rebec, T. Jia, M. Hashimoto, D. Lu, B. Moritz, R. G. Moore, T. P. Devereaux, and Z.-X. Shen, *Science* **373**, 1235 (2021).
- [63] Y. Wang, Z. Chen, T. Shi, B. Moritz, Z.-X. Shen, and T. P. Devereaux, arXiv:2107.05773 (2021).
- [64] F. Görg, M. Messer, K. Sandholzer, G. Jotzu, R. Desbuquois, and T. Esslinger, *Nature* **553**, 481 (2018).
- [65] M. Messer, K. Sandholzer, F. Görg, J. Minguzzi, R. Desbuquois, and T. Esslinger, *Phys. Rev. Lett.* **121**, 233603 (2018).
- [66] K. Sandholzer, Y. Murakami, F. Görg, J. Minguzzi, M. Messer, R. Desbuquois, M. Eckstein, P. Werner, and T. Esslinger, *Phys. Rev. Lett.* **123**, 193602 (2019).
- [67] K. Viebahn, J. Minguzzi, K. Sandholzer, A.-S. Walter, M. Sajnani, F. Görg, and T. Esslinger, *Phys. Rev. X* **11**, 011057 (2021).
- [68] P. Sengupta, A. W. Sandvik, and D. K. Campbell, *Phys. Rev. B* **65**, 155113 (2002).
- [69] E. Jeckelmann, *Phys. Rev. Lett.* **89**, 236401 (2002).
- [70] Y. Z. Zhang, *Phys. Rev. Lett.* **92**, 246404 (2004).
- [71] A. W. Sandvik, L. Balents, and D. K. Campbell, *Phys. Rev. Lett.* **92**, 236401 (2004).
- [72] S. Ejima and S. Nishimoto, *Phys. Rev. Lett.* **99**, 216403 (2007).
- [73] M. Dalmonte, J. Carrasquilla, L. Taddia, E. Ercolessi, and M. Rigol, *Phys. Rev. B* **91**, 165136 (2015).
- [74] J. Spalding, S.-W. Tsai, and D. K. Campbell, *Phys. Rev. B* **99**, 195445 (2019).
- [75] H. Q. Lin, D. K. Campbell, and R. T. Clay, *Chin. J. Phys.* **38**, 1 (2000).
- [76] F. Heidrich-Meisner, M. Rigol, A. Muramatsu, A. E. Feiguin, and E. Dagotto, *Phys. Rev. A* **78**, 013620 (2008).
- [77] F. Heidrich-Meisner, S. R. Manmana, M. Rigol, A. Muramatsu, A. E. Feiguin, and E. Dagotto, *Phys. Rev. A* **80**, 041603 (2009).
- [78] D. Karlsson, C. Verdozzi, M. M. Odashima, and K. Capelle, *EPL (Europhysics Letters)* **93**, 23003 (2011).
- [79] J. Kajala, F. Massel, and P. Törmä, *Phys. Rev. Lett.* **106**, 206401 (2011).
- [80] S. Keßler, A. Holzner, I. P. McCulloch, J. von Delft, and F. Marquardt, *Phys. Rev. A* **85**, 011605 (2012).
- [81] S. Langer, M. J. A. Schuetz, I. P. McCulloch, U. Schollwöck, and F. Heidrich-Meisner, *Phys. Rev. A* **85**, 043618 (2012).
- [82] C.-C. Chien, M. Zwolak, and M. Di Ventura, *Phys. Rev. A* **85**, 041601 (2012).
- [83] S. Keßler, I. P. McCulloch, and F. Marquardt, *New Journal of Physics* **15**, 053043 (2013).
- [84] L. Vidmar, S. Langer, I. P. McCulloch, U. Schneider, U. Schollwöck, and F. Heidrich-Meisner, *Phys. Rev. B* **88**, 235117 (2013).
- [85] D. Lacroix, S. Hermanns, C. M. Hinz, and M. Bonitz, *Phys. Rev. B* **90**, 125112 (2014).
- [86] Z. Mei, L. Vidmar, F. Heidrich-Meisner, and C. J. Bolech, *Phys. Rev. A* **93**, 021607 (2016).
- [87] N. Schlünzen, J.-P. Joost, F. Heidrich-Meisner, and M. Bonitz, *Phys. Rev. B* **95**, 165139 (2017).
- [88] M. W. Cook and S. R. Clark, *Phys. Rev. A* **101**, 033604 (2020).
- [89] R. Rausch and M. Potthoff, *Phys. Rev. B* **95**, 045152 (2017).
- [90] T. Enss and J. Sirker, *New J. Phys.* **14**, 023008 (2012).
- [91] A. Bauer, F. Dorfner, and F. Heidrich-Meisner, *Phys. Rev. A* **91**, 053628 (2015).
- [92] S. A. Hamerla and G. S. Uhrig, *Phys. Rev. B* **87**, 064304 (2013).
- [93] K. Ido, T. Ohgoe, and M. Imada, *Phys. Rev. B* **92**, 245106 (2015).
- [94] P. Bleicker and G. S. Uhrig, *Phys. Rev. A* **98**, 033602 (2018).
- [95] F. Goth and F. F. Assaad, *Phys. Rev. B* **85**, 085129 (2012).
- [96] I. G. White, R. G. Hulet, and K. R. A. Hazzard, *Phys. Rev. A* **100**, 033612 (2019).
- [97] F. Hofmann and M. Potthoff, *Phys. Rev. B* **85**, 205127 (2012).
- [98] C. Shao, T. Tohyama, H.-G. Luo, and H. Lu, *Phys. Rev. B* **101**, 045128 (2020).
- [99] S. Paeckel, B. Fauseweh, A. Osterkorn, T. Köhler, D. Manske, and S. R. Manmana, *Phys. Rev. B* **101**, 180507 (2020).
- [100] G. Vidal, *Phys. Rev. Lett.* **93**, 040502 (2004).
- [101] S. Paeckel, T. Köhler, A. Swoboda, S. R. Manmana, U. Schollwöck, and C. Hubig, *Annals of Physics* **411**, 167998 (2019), ISSN 0003-4916.
- [102] S. Al-Assam, S. R. Clark, D. Jaksch, and T. Development Team, *Tensor Network Theory Library, Beta Version 1.2.0* (2016), URL <http://www.tensornetworktheory.org>.
- [103] S. Al-Assam, S. R. Clark, and D. Jaksch, *J. Stat. Mech.* **2017**, 093102 (2017).
- [104] J. R. Schrieffer and P. A. Wolff, *Phys. Rev.* **149**, 491 (1966).
- [105] K. Yang, L. Zhou, W. Ma, X. Kong, P. Wang, X. Qin, X. Rong, Y. Wang, F. Shi, J. Gong, et al., *Phys. Rev. B* **100**, 085308 (2019).
- [106] S. Zamani, R. Jafari, and A. Langari, *Phys. Rev. B* **102**, 144306 (2020).
- [107] R. Jafari and A. Akbari, *Phys. Rev. A* **103**, 012204 (2021).
- [108] L. Zhou and Q. Du, *Journal of Physics: Condensed Matter* **33**, 345403 (2021), URL <https://doi.org/10.1088/1361-648x/ac0b60>.
- [109] R. Hamazaki, *Nat. Commun.* **12**, 5108 (2021).
- [110] N. Tsuji, T. Oka, P. Werner, and H. Aoki, *Phys. Rev. Lett.* **106**, 236401 (2011).
- [111] J. J. Mendoza-Arenas, F. J. Gómez-Ruiz, M. Eckstein, D. Jaksch, and S. R. Clark, *Ann. Phys. (Berlin)* **529**, 1700024 (2017).
- [112] M. H. Kalthoff, D. M. Kennes, and M. A. Sentef, *Phys. Rev. B* **100**, 165125 (2019).
- [113] A. J. Daley, H. Pichler, J. Schachenmayer, and P. Zoller, *Phys. Rev. Lett.* **109**, 020505 (2012).
- [114] H. Pichler, L. Bonnes, A. J. Daley, A. M. Läuchli, and P. Zoller, *New J. Phys.* **15**, 020505 (2013).
- [115] K. Singh, C. J. Fujiwara, Z. A. Geiger, E. Q. Simmons, M. Lipatov, A. Cao, P. Dotti, S. V. Rajagopal, R. Senaratne, T. Shimasaki, et al., *Phys. Rev. X* **9**, 041021 (2019).
- [116] S. Sugawa, K. Inaba, S. Taie, R. Yamazaki, M. Yamashita, and Y. Takahashi, *Nat. Phys.* **7**, 642 (2011).
- [117] I. Ferrier-Barbut, M. Delehaye, S. Laurent, A. T. Grier, M. Pierce, B. S. Rem, F. Chevy, and C. Salomon, *Science* **345**, 1035 (2014).
- [118] R. S. Lous, I. Fritsche, M. Jag, F. Lehmann, E. Kirilov, B. Huang, and R. Grimm, *Phys. Rev. Lett.* **120**, 243403 (2018).

- (2018).
- [119] M. Gärttner, A. Safavi-Naini, J. Schachenmayer, and A. M. Rey, *Phys. Rev. A* **100**, 053607 (2019).
 - [120] J. J. Mendoza-Arenas and B. Buča, arXiv:2106.06277 (2021).
 - [121] M. Bukov, M. Kolodrubetz, and A. Polkovnikov, *Phys. Rev. Lett.* **116**, 125301 (2016).
 - [122] We note that the DQPTs of Ref. [19] appear at twice

the times of our critical times, since their hopping is half of ours. Also, our rate function is twice as large since we have the components of spin up and down orientations. Finally, the small peaks after the second DQPT in Fig. 6(a) correspond to finite size effects, strongly reduced as L is increased, as we verified with simulations of different system sizes.